# APPLICATION OF ELASTIC FOUNDATION BEAMS IN COMPOSITE FRACTURE MECHANICS - ANALYSIS OF THE ELS SPECIMEN

**András Szekrényes***, **József Uj****
Department of Applied Mechanics, Budapest University of Technology and Economics, 1111, Budapest, Muegyetem rkp. 5., Hungary
PhD Student*, Tel: +36 1 463 1170, E-mail: szeki@mm.bme.hu
Associate Professor**, Tel: +36 1 463 2228, E-mail: uj@mm.bme.hu

***Summary***

*The mixed-mode I/II interlaminar fracture in glass/polyester composite ELS specimens was investigated analytically and experimentally. Advanced compliance and fracture energy equations were developed based on higher order beam theories. Quasi-unidirectional glass/polyester specimens were manufactured and tested. Beam equations were compared with experimental results in a long crack interval and agreed quite closely.*

## 1 INTRODUCTION

Delamination tests have important role in the development of composite structures. The mixed-mode I+II delamination can be investigated by using the ELS (end-loaded split) specimen (see Fig.1). In literature only the result of the simple beam theory was found. In the current study beam theories were utilized to derive compliance and fracture energy equations for the ELS specimen. The equations incorporate elastic foundation, Saint Venant effect [1] and crack tip deformation analysis based on [2]. Unidirectional glass/polyester specimens were manufactured and tested. Experiments were carried out to check the deduced equations. Results show excellent correspondence between analysis and experiment.

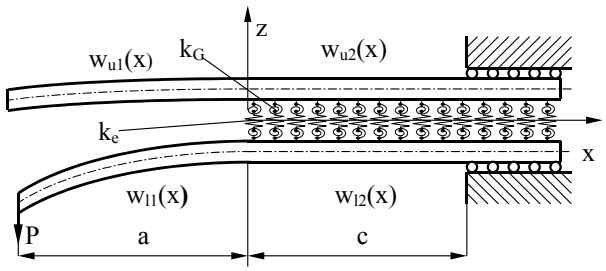


**Fig.1.** Two-parameter elastic foundation model

## 2 BEAM ANALYSIS

### 2.1 Winkler-Pasternak foundation analysis

The governing ODE system of the two-parameter elastic foundation model depicted in Fig.1.:

$$\frac{d^4 w_{l2}(x)}{dx^4} - 2\psi^4 \frac{d^2 w_{l2}(x)}{dx^2} + 4\beta^4 w_{l2}(x) = -2\psi^4 \frac{d^2 w_{u2}(x)}{dx^2} + 4\beta^4 w_{u2}(x),\ 0 \le x \le c, \qquad (1)$$

$$\frac{d^4 w_{u2}(x)}{dx^4} - 2\psi^4 \frac{d^2 w_{u2}(x)}{dx^2} + 4\beta^4 w_{u2}(x) = -2\psi^4 \frac{d^2 w_{l2}(x)}{dx^2} + 4\beta^4 w_{l2}(x),\ 0 \le x \le c,$$

where β, ψ can be associated to elastic moduli of the specimen:

$$\beta = \left(\frac{3}{4}\right)^{\frac{1}{4}} \frac{1}{h}\left(\frac{E_{33}}{E_{11}}\right)^{\frac{1}{4}}, \quad \psi = \left(\frac{3}{4}\right)^{\frac{1}{4}} \frac{1}{h^{\frac{1}{2}}}\left(\frac{G_{13}}{E_{11}}\right)^{\frac{1}{4}}. \qquad (2)$$

The characteristic roots of the ODE system:

$$m_{41}=\sqrt{\sqrt{2}\beta^2-\psi^4}\,, \qquad m_{42}=\sqrt{\sqrt{2}\beta^2+\psi^4}\,. \tag{3}$$

The solution functions of the uncracked ( $0\le x\le c$ ) part can be formulated as:

$$\begin{aligned} w_{l2}(x) &= c_1+c_2x+c_3x^2+c_4x^3+[c_5\cos(m_{41}x)+c_6\sin(m_{41}x)]\mathrm{ch}(m_{42}x)+ \\ &\quad +[c_7\cos(m_{41}x)+c_8\sin(m_{41}x)]\mathrm{sh}(m_{42}x) \\ w_{u2}(x) &= c_1+c_2x+c_3x^2+c_4x^3-[c_5\cos(m_{41}x)+c_6\sin(m_{41}x)]\mathrm{ch}(m_{42}x)+ \\ &\quad -[c_7\cos(m_{41}x)+c_8\sin(m_{41}x)]\mathrm{sh}(m_{42}x) \end{aligned}, \tag{4}$$

For the upper and lower arms of the specimen the deflection functions are:

$$w_{u1}(x)=c_9x+c_{10}, \qquad w_{l1}(x)=-\frac{P[x^3/6+ax^2/2]}{I^l_{y1}E_{11}}+c_{11}x+c_{12}, \qquad -a\le x\le 0. \tag{5}$$

The boundary conditions can be written as: $w_{u2}(c)=0$, $w_{l2}(c)=0$, $w'_{u2}(c)=0$, $w'_{l2}(c)=0$. The matching conditions: $w_{u1}(0)=w_{u2}(0)$, $w_{l1}(0)=w_{l2}(0)$, $w'_{u1}(0)=w'_{u2}(0)$, $w'_{l1}(0)=w'_{l2}(0)$, $w''_{u1}(0)=4w''_{u2}(0)$, $w''_{l1}(0)=4w''_{l2}(0)$, $w'''_{u1}(0)=4w'''_{u2}(0)$, $w'''_{l1}(0)=4w'''_{l2}(0)$. After some meaningful simplification we can obtain the compliance of the ELS specimen ($C=w_{l1}(-a)/P$):

$$C=\frac{7a^3+L^3}{2bh^3E_{11}}+\frac{a^3}{2bh^3E_{11}}\left[2.71\left(\frac{h}{a}\right)\left(\frac{E_{11}}{E_{33}}\right)^{\frac{1}{4}}\phi^{\frac{1}{2}}+2.45\left(\frac{h}{a}\right)^2\left(\frac{E_{11}}{E_{33}}\right)^{\frac{1}{2}}\phi+1.11\left(\frac{h}{a}\right)^3\left(\frac{E_{11}}{E_{33}}\right)^{\frac{3}{4}}\phi^{\frac{1}{2}}\right], \tag{6}$$

where $L=a+c$ is the specimen length and: $\phi=1+\frac{\psi^4}{\sqrt{2}\beta^2}=1+\frac{1}{2}\left(\frac{3}{2}\right)^{\frac{1}{2}}\frac{G_{13}}{\sqrt{E_{11}E_{33}}}$. (7)

### 2.2 Saint Venant effect

The problem of Saint Venant effect (illustrated in Fig.2) was analysed by Olsson [1] for the DCB specimen. According to [1] the compliance contribution has the following form in the case of the ELS specimen:

$$C_{SV}=\frac{3}{\pi}\frac{L^2}{bh^2E_{11}}\left(\frac{E_{11}}{G_{13}}\right)^{\frac{1}{2}}. \tag{8}$$

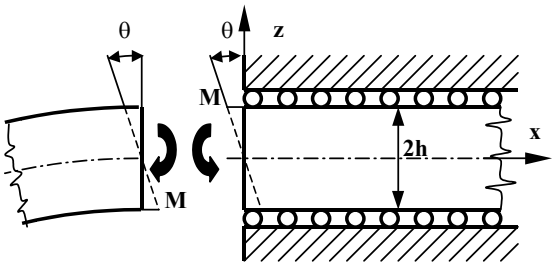


**Fig.2.** Saint Venant effect at the clamped end

According to Eq.(8) the Saint Venant effect is independent on the crack length.

### 2.3 Crack tip deformation analysis

According to Wang et al. [2] the governing ODE of the shear stress field in the uncracked region and its approximate solution is:

$$\frac{d^2\tau}{dx^2}-\frac{21\lambda G_{13}}{4h^2E_{11}}\tau=0, \quad \tau(x)=-\frac{3}{4}\frac{P}{b\chi h^2}e^{-\frac{x-a}{\chi h}}, \ \chi=\left(\frac{4E_{11}}{21\lambda G_{13}}\right)^{\frac{1}{2}}, \tag{9}$$

where $\lambda$ is the correction due to orthotropy, we choose $\lambda=1$. The deflections of the uncracked ($w(x)$) and cracked ($w_0(x)$) regions follow by integrating the stress field:

$$w(x)=-\frac{3}{8}\frac{Pa(\chi h)^2}{I_yE_{11}}e^{-\frac{x-a}{\chi h}}+c_1x+c_2, \quad w_0(x)=-\frac{Px^3}{16I_{y0}E_{11}}+c_3x+c_4. \tag{10}$$

Boundary and matching conditions are necessary to determine all the four constants: $w(L)=0$, $w'(L)=0$, $w_0(a)=w(a)$, $w'_0(a)=w'(a)$. The compliance (again after some simplification) is:

$$C=\frac{3a^3}{8bh^3E_{11}}[4+3\chi\left(\frac{h}{a}\right)+3\chi^2\left(\frac{h}{a}\right)^2]. \tag{11}$$

### 2.4 Summing the compliance and fracture energy contributions

As the superposition of the derived equations the compliance of the ELS specimen has the following form (by adding Eq.(6), Eq.(8) and Eq.(11)):

$$C=\frac{7a^3+L^3}{2bh^3E_{11}}+\frac{a^3}{2bh^3E_{11}}[2.71\left(\frac{h}{a}\right)\left(\frac{E_{11}}{E_{33}}\right)^{\frac{1}{4}}\phi^{\frac{1}{2}}+2.45\left(\frac{h}{a}\right)^2\left(\frac{E_{11}}{E_{33}}\right)^{\frac{1}{2}}\phi+1.11\left(\frac{h}{a}\right)^3\left(\frac{E_{11}}{E_{33}}\right)^{\frac{3}{4}}\phi^{\frac{1}{2}}]+$$
$$+\frac{3}{\pi}\frac{L^2}{bh^2E_{11}}\left(\frac{E_{11}}{G_{13}}\right)^{\frac{1}{2}}+\frac{a^3}{2bh^3E_{11}}[0.98\left(\frac{h}{a}\right)\left(\frac{E_{11}}{\lambda G_{13}}\right)^{\frac{1}{2}}+0.43\left(\frac{h}{a}\right)^2\left(\frac{E_{11}}{\lambda G_{13}}\right)] \tag{12}$$

The fracture energy can be obtained by using the Irwin-Kies expression [1]:

$$G_{I+II}=\frac{21P^2a^2}{4b^2h^3E_{11}}+\frac{P^2a^2}{4b^2h^3E_{11}}[5.42\left(\frac{h}{a}\right)\left(\frac{E_{11}}{E_{33}}\right)^{\frac{1}{4}}\phi^{\frac{1}{2}}+2.45\left(\frac{h}{a}\right)^2\left(\frac{E_{11}}{E_{33}}\right)^{\frac{1}{2}}\phi]+$$
$$+\frac{P^2a^2}{4b^2h^3E_{11}}[1.96\left(\frac{h}{a}\right)\left(\frac{E_{11}}{\lambda G_{13}}\right)^{\frac{1}{2}}+0.43\left(\frac{h}{a}\right)^2\left(\frac{E_{11}}{\lambda G_{13}}\right)] \tag{13}$$

### 2.5 Mode-mixity analysis

In order to separate the total strain energy release rate ($G_{I+II}$) into its individual components ($G_I$, $G_{II}$) we use again higher order beam theories. We complete the global [3] and local [4] methods with foundation effects.

#### *2.5.1 Global method*

If we complete the global method [3] with foundation effects (Winkler-Pasternak, shear deformation of the crack tip) we can obtain the mode-I and mode-II components:

$$G_I=\frac{M_I^2(12+f_{W2})}{b^2h^3E_{11}},\quad f_{W2}=5.42\left(\frac{h}{a}\right)\left(\frac{E_{11}}{E_{33}}\right)^{\frac{1}{4}}\phi^{\frac{1}{2}}+2.45\left(\frac{h}{a}\right)^2\left(\frac{E_{11}}{E_{33}}\right)^{\frac{1}{2}}\phi, \tag{14}$$

$$G_{II}=\frac{M_{II}^2(9+f_{SH})}{b^2h^3E_{11}},\quad f_{SH}=1.962\left(\frac{h}{a}\right)\left(\frac{E_{11}}{\lambda G_{13}}\right)^{\frac{1}{2}}+0.428\left(\frac{h}{a}\right)^2\left(\frac{E_{11}}{\lambda G_{13}}\right). \tag{15}$$

According to this analysis the Winkler-Pasternak foundation contributes only to the mode-I component, while crack tip deformation due to shear stresses supports the mode-II fracture energy. The mode-I and mode-II bending moments according to [3]:

$$M_I=(M_1-M_2)/2,\quad M_{II}=(M_1+M_2)/2. \tag{16}$$

For the ELS specimen $M_1=0$, $M_2=Pa$ are reduced moments at the crack tip, we obtain by the help of Eq.(14) and (15)

$$G_I=\frac{12P^2a^2}{4b^2h^3E_{11}}[1+0.451\left(\frac{h}{a}\right)\left(\frac{E_{11}}{E_{33}}\right)^{\frac{1}{4}}\phi^{\frac{1}{2}}+0.204\left(\frac{h}{a}\right)^2\left(\frac{E_{11}}{E_{33}}\right)^{\frac{1}{2}}\phi], \tag{17}$$

$$G_{II}=\frac{9P^2a^2}{4b^2h^3E_{11}}[1+0.218\left(\frac{h}{a}\right)\left(\frac{E_{11}}{\lambda G_{13}}\right)^{\frac{1}{2}}+0.048\left(\frac{h}{a}\right)^2\left(\frac{E_{11}}{\lambda G_{13}}\right)]. \tag{18}$$

*2.5.2 Local method*

The local method is based on the work of Suo and Hutchinson [4]. The energy release rate components supposing plane stress conditions:

$$G_I = \frac{1}{2b^2 E_{11}}\left[\frac{F}{\sqrt{Ah}}\cos(\omega) \pm \frac{M}{\sqrt{Bh^3}}\sin(\omega+\gamma)\right]^2, \tag{19}$$

$$G_{II} = \frac{1}{2b^2 E_{11}}\left[\frac{F}{\sqrt{Ah}}\sin(\omega) \mp \frac{M}{\sqrt{Bh^3}}\cos(\omega+\gamma)\right]^2, \tag{20}$$

where:

$$A = \frac{18}{252 + 9f_{W2} + 16f_{SH}}, \qquad B = \frac{1}{2}\frac{1}{(12+f_{W2})}, \qquad \gamma = \arcsin[\sqrt{AB}(12+f_{W2})], \tag{21}$$

$$\omega = \frac{\pi}{180}49.1, \quad F = \frac{3}{4}\frac{(M_1+M_2)}{h}, \qquad M = \frac{7M_1 - M_2}{8}, \tag{22}$$

where the upper sign is for case of $FM>0$, and the lower sign is for $FM<0$. Eq.(21) incorporates the effect of elastic foundations.

## 3 EXPERIMENTS

Experiments were carried out using the special fixture depicted in Fig.3. The specimen displacement was measured by the dial gauge also shown in Fig.3. Specimens with different crack lengths were used and loaded up to fracture. The compliance calibration method [3] was used as data reduction scheme. This procedure resulted only initiation fracture energies. The flexural properties: $E_{11}$=33 GPa, $G_{13}$=3 GPa, $E_{33}$=7.2 GPa.

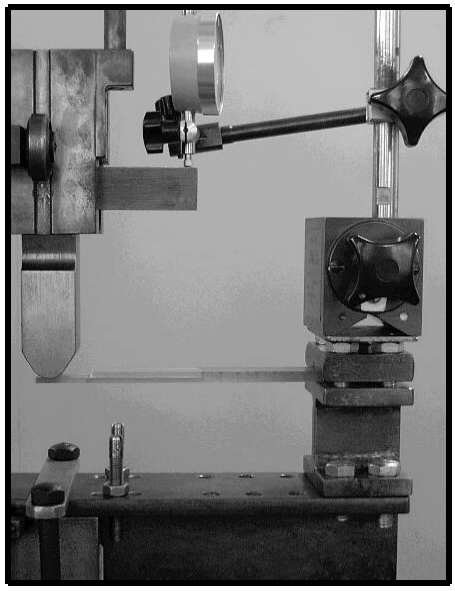

**Fig. 3.** Experimental setup

## 4 RESULTS AND DISCUSSION

During testing linear load-specimen displacement curves were recorded for each specimen as shown by Fig.4. The compliance and fracture energy curves are depicted in Fig.5. The advanced beam model [Eq.(12)] shows excellent correspondence with the experiments. Fracture energy curves can also be seen in Fig.5.b. Experiments produced approximate steady state value of $G_{I+II}$=645 J/m$^2$, while beam analysis resulted $G_{I+II}$=573 J/m$^2$. The results of mode-mixity analysis (Fig.5.b) show that the global and local methods give exactly the same mode components. Both methods report mode-I dominance. The contributions of the various effects are collected in Tab.1. The compliance contribution of Winkler-Pasternak foundation has

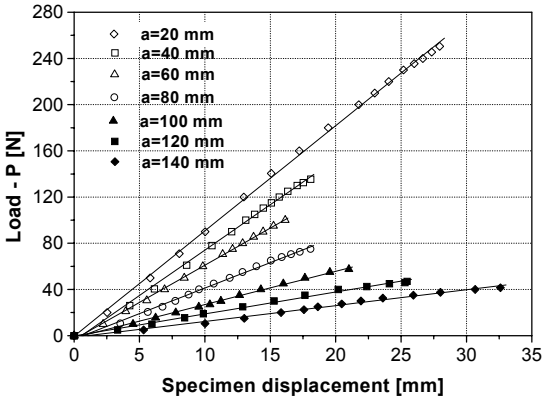


**Fig. 4.** Load-specimen displacement curves up to fracture initiation

reasonable values only for long crack lengths, while fracture energy is supported mainly in short crack lengths. The crack tip shear deformation has the same behavior as can be seen in Tab.1. The Saint Venant effect produces a reasonable constant compliance term, which is necessary to predict the compliance with more accuracy.

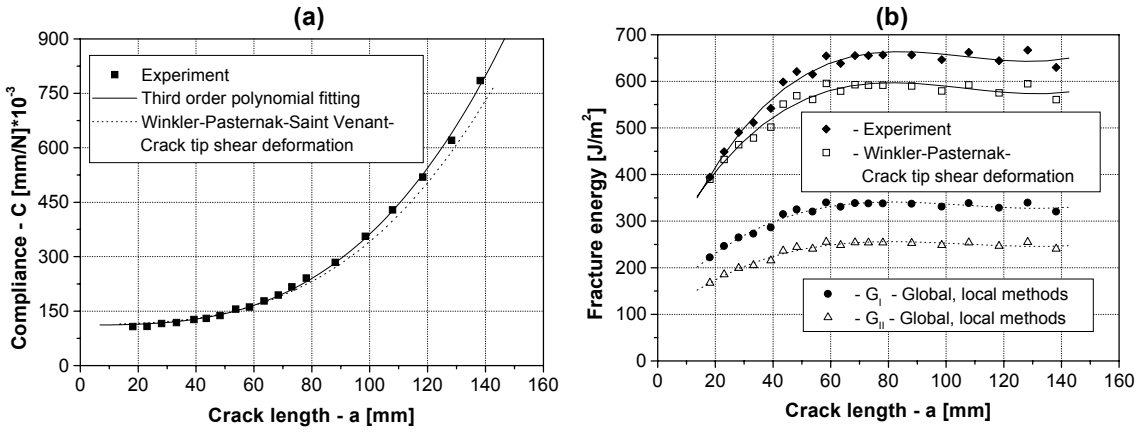


**Fig. 5.** Specimen compliance (a) and critical values of the initiation fracture energy (b) against the crack length

## 4 CONCLUSIONS

Beam analysis resulted a full third order polynomial for the ELS specimen compliance, fracture energy was also calculated. Experiment was carried out on glass/polyester specimens in order to verify the new equations and produced excellent correspondence with the analysis. Global and local mode-mixity analysis incorporating foundation effects provided the same mode components and reported mode-I dominance.

| a [mm] | $C_{SB}$ | $C_{W-P}$ | $C_{SV}$ | $C_{SH}$ | $G_{I+II,SB}$ | $G_{I+II,W-P}$ | $G_{I+II,SH}$ |
|---|---|---|---|---|---|---|---|
| | [mm/N]·10^-3 | | | | [J/m^2] | | |
| 20 | 102.71 | 0.16 | 12.65 | 0.12 | 345.79 | 24.70 | 19.24 |
| 30 | 106.80 | 0.35 | 12.69 | 0.27 | 430.21 | 19.08 | 14.84 |
| 40 | 115.51 | 0.65 | 12.72 | 0.51 | 475.50 | 14.81 | 11.51 |
| 60 | 146.03 | 1.40 | 12.71 | 1.10 | 574.48 | 11.82 | 9.18 |
| 100 | 311.37 | 3.87 | 12.67 | 3.00 | 567.34 | 6.84 | 5.31 |
| 140 | 680.33 | 7.53 | 12.62 | 5.84 | 552.59 | 4.72 | 3.66 |

$C_{SB}$, $G_{I/II,SB}$ - contribution of simple beam theory
$C_{W-P}$, $G_{I/II,W-P}$ - contribution of Winkler-Pasternak elastic foundation
$C_{SV}$ - contribution of Saint Venant effect
$C_{SH}$, $G_{I/II,SH}$ - contribution of crack tip shear deformation

**Tab.1**. Compliances and fracture energies by beam analysis

## REFERENCES


1. Olsson R. (1992), "A simplified improved beam analysis of the DCB specimen", *Composites Science and Technology*, Vol 43, 329-338.
2. Wang J, Qiao P. (2004), " Novel beam analysis of the end notched flexure specimen for mode-II fracture", *Engineering Fracture Mechanics*, Vol. 71, 219-231.
3. Ducept F., Gamby D., Davies P. (1999), "A mixed-mode failure criterion derived from tests of symmetric and asymmetric specimens", *Composites Science and Technology*, Vol. 59, 609-619.
4. Dahlen C., Springer G.S., (1994), "Delamination growth in composites under cyclic loads", *Journal of Composite Materials*, Vol. 28, 732-781.